Chaotic dynamics of a magnetic particle at finite temperature

O. J. Suarez,[1,2] D. Laroze,[1,*] J. Martínez-Mardones,[3] D. Altbir,[4] and O. Chubykalo-Fesenko[5]
[1]*Instituto de Alta Investigación, Universidad de Tarapacá, Casilla 7D, Arica, Chile*
[2]*Departamento de Física, Universidad de Sucre, A.A. 406, Sincelejo, Colombia*
[3]*Instituto de Física, Pontificia Universidad Católica de Valparaíso, Casilla 4059, Valparaíso, Chile*
[4]*Departamento de Física, CEDENNA, Universidad de Santiago de Chile, Avenida Ecuador 3493, Santiago, Chile*
[5]*Instituto de Ciencia de Materiales, Consejo Superior de Investigaciones Científicas, Cantoblanco, E-28049 Madrid, Spain*
(Received 16 June 2016; revised manuscript received 16 November 2016; published 6 January 2017)

In this work, we study nonlinear aspects of the deterministic spin dynamics of an anisotropic single-domain magnetic particle at finite temperature modeled by the Landau-Lifshitz-Bloch equation. The magnetic field has two components: a constant term and a term involving a harmonic time modulation. The dynamical behavior of the system is characterized with the Lyapunov exponents and by means of bifurcation diagrams and Fourier spectra. In particular, we explore the effects of the magnitude and frequency of the applied magnetic field, finding that the system presents multiple transitions between regular and chaotic states when varying the control parameters. We also address the temperature dependence and evidence that it plays an important role in these transitions, almost suppressing the chaotic behavior close to the Curie temperature. Finally, we find that the system has hyperchaotic states for specific values of field and temperature.

DOI: 10.1103/PhysRevB.95.014404

I. INTRODUCTION

Following the advances in pump-probe techniques, in recent decades, fast magnetization dynamics has become experimentally observable on the time scale below 10 ns [1,2]. This has allowed the generation of dynamic studies of the precession of magnetization and switching of magnetic dots [1–4]. With more powerful femtosecond lasers, the manipulation and switching of the magnetization at even the femto- and picosecond scales have become a reality [5–9]. These experimental advances have triggered new studies on the spin dynamics of ferromagnets, allowing one to explore novel dynamical scenarios. From both applied and theoretical points of view, it is important to understand the peculiarities of the dynamics of magnetic nanoparticles. Even in the simplest single-domain limit, this dynamics is expected to be highly nontrivial due to the nonlinear character of the Landau-Lifshitz-Gilbert (LLG) equation of motion [10]. For example, the dynamical precessional switching under microwave excitation can take place under fields below the Stoner-Wolfarth limit due to nonlinear effects [11] and may result in very complex trajectories of the magnetization [12]. Another example is highly nonlinear trajectories and states, which have been reported in the dynamics of nanosized spin valves [13,14]. In this context, a number of numerical studies of nonlinear dynamics and of the effect of time-dependent magnetic fields have been developed [12,15–31], reporting different dynamical behaviors such as quasiperiodicity, bistability, and chaos [15]. Such effects have been analyzed using different approaches such as the Lyapunov exponents [25–28], bifurcation diagrams [15,24], Fourier spectra [25–28], and Hausdorff dimension [31]. From the experimental point of view, several chaotic states have been measured [32–35]. The usual magnetic elements are yttrium iron garnet spheres [32]. Different routes to chaos have been found using ferromagnetic resonance methods. In particular, period-doubling cascades, quasiperiodic routes to chaos, or intermittent routes can be appear. This implies that there is no universal mechanism leading to chaos in a magnetic system, and therefore theoretical and numerical studies are necessary and in order. The study of the chaotic states is also important from an applied point of view since they can potentially lead to a broad emission spectrum of radio-frequency oscillators based on the spin-torque effect, and the transition between deterministic and chaotic states can also be important for radio-frequency detectors; see, e.g., [36]. Finally, the standard application of chaos is in cryptography devices; see, e.g., [37].

The ultrafast magnetization experiments have opened the possibility to study not only transverse but also longitudinal magnetization dynamics [5–9]. Recently, a deterministic differential equation that describes the magnetization dynamics at finite temperatures and accounts for longitudinal dynamics was derived by Garanin from both the quantum and the classical nonequilibrium statistical mechanics points of view [38–40]. This equation is usually called the Landau-Lifshitz-Bloch (LLB) equation. In this model, the temperature induces changes in the module of the magnetization and, therefore, the magnetization magnitude is not conserved [39]. It was demonstrated that the LLB equation is effective to properly estimate the longitudinal and transversal relaxation times predicted by atomistic simulations at high temperatures [41]. Furthermore, the LLB equation is in agreement with several experimental measurements of ultrafast dynamics [42–45]. Other interesting works in the wide range of magnetic-thermal phenomena where the LLB model is involved have been published [46–53]. For example, and just to mention a few, LLB has been used for modeling heat-assisted magnetic recording [50,51], or the thermal induction of domain-wall motion under the spin Seebeck effect [48].

From the dynamical system point of view, the main difference between the LLG and the LLB equations is that in the first one, the magnetization length is conserved, and therefore undamped LLG has a constant of motion [10]. The

*dlarozen@uta.cl

LLB model has an extra degree of freedom and, consequently, one can expect more complex dynamical behaviors. Particularly, the appearance of one more degree of freedom may drug the system from a regular to a chaotic regime. Furthermore, the ultrafast magnetization switching phenomena in ferrimagnets have been analyzed within the LLB model as arising from highly nonlinear trajectories involving the angular momentum transfer from pure longitudinal to transverse motion [52].

In this paper, we focus on an anisotropic single-domain magnetic particle in the presence of a magnetic field with constant and time-dependent terms at finite temperature. In our study, we use the LLB equation that allows us to clarify the effects of the temperature and the external magnetic field on the system. The paper is organized as follows: In Sec. II, the LLB equation and the mean-field approximation to account for temperature-dependent properties are presented. In Sec. III, numerical results of the Lyapunov spectra, bifurcation diagrams, phase portraits, and Fourier power spectra are shown and analyzed. Finally, conclusions are presented in Sec. IV.

II. THEORETICAL MODEL

Let us consider an anisotropic magnetic particle at finite temperature T. We assume that the particle is in a magnetic monodomain state $\mathbf{M}$ (i.e., the *macrospin* approximation), which means that we do not consider long-wave spatial magnetization inhomogeneities such as domain walls. In this case, the temporal evolution of the magnetization is governed by the LLB equation, which in a dimensionless form is given by [38,39]

$$\frac{d\mathbf{m}}{d\tau} = -\mathbf{m}\times\Gamma - \frac{\alpha_\perp}{m^2}\mathbf{m}\times(\mathbf{m}\times\Gamma) + \frac{\alpha_\parallel}{m^2}(\mathbf{m}\cdot\Gamma)\mathbf{m}, \quad (1)$$

where $\mathbf{m} = \mathbf{M}/M_0$, with M_0 the saturation magnetization at zero temperature, and $\tau = t|\gamma|/\mu_0\tilde{\chi}_\perp^0$ is the normalized time. In this expression, $\tilde{\chi}_\perp^0$ is the transversal magnetic susceptibility at zero temperature $(\partial m/\partial H)_{H\longrightarrow 0}$ (defined by the anisotropy constant), $|\gamma|$ represents the gyromagnetic factor, μ_0 is the vacuum magnetic permeability, with $|\gamma| = |\gamma_e|\mu_0 \approx 2.21\times 10^5$ m A^{-1}s^{-1}. In Eq. (1), $\Gamma = \mu_0\tilde{\chi}_\perp^0\mathbf{H}_{\rm eff}$ denotes the dimensionless effective field, and $\alpha_\perp(T)$ and $\alpha_\parallel(T)$ are the transverse and longitudinal damping coefficients, respectively. These coefficients are temperature dependent and their form depends on the quantum spin number S [40]. When $T\to 0$, $\alpha_\parallel\to 0$ and the transverse damping coefficient tends to the standard Gilbert damping coefficient ($\alpha_\perp\to\alpha_0$). Consequently, the last term on the right-hand side of Eq. (1) represents a torque that appears only from temperature effects. Therefore, when $T\to 0$, the LLB equation is reduced to the Landau-Lifshitz (LL) equation [10],

$$\frac{d\mathbf{m}}{d\tau} = -\mathbf{m}\times\Gamma - \alpha_0\mathbf{m}\times\mathbf{m}\times\Gamma. \quad (2)$$

Note that in the LLG equation, the module of the magnetic moment is conserved. Nevertheless, in the LLB, this condition is removed and a longitudinal degree of freedom appears, allowing changes on the module of the magnetic moment generating a more complex dynamic. In addition, let us remark that the thermal effects are included here on average. In the classical approach, the magnetization $\mathbf{M}$ represents the statistical average of the fluctuating atomistic spins [39], while in the quantum approach, it represents the spin expectation value [38]. The thermal fluctuations may be additionally included as stochastic fields in the LLB equation [54], similar to the standard macroscopic approach in the LLG [55–57]. This represent a way to thermally excite the system; however, this does not change the system's linear (spin waves) or nonlinear excitations. The macrospin LLB deterministic approach has been compared to atomistic Langevin simulations in different situations given very good agreements [41], and also has been used to complement the computation of magnetic properties of complex materials [51].

Here we assume that the temperature is less than the Curie temperature T_C. In this scenario, the effective magnetic field Γ can be written as [39]

$$\Gamma = \mathbf{h}_E - \frac{1}{\tilde{\chi}_\perp}\left(m_x\hat{\mathbf{x}} + m_y\hat{\mathbf{y}}\right) + \frac{\tilde{\chi}_\perp^0}{2\tilde{\chi}_\parallel}\left(1 - \frac{m^2}{m_e^2}\right)\mathbf{m}, \quad (3)$$

where $\mathbf{h}_E$ is an external magnetic field, $\tilde{\chi}_\perp(T)$ and $\tilde{\chi}_\parallel(T)$ are the perpendicular and parallel susceptibilities, respectively, and $m_e(T)$ is the equilibrium magnetization. The external field contains a constant and a harmonic time-dependent term,

$$\mathbf{h}_E = h_z\hat{\mathbf{z}} + h_x\sin(\Omega\tau)\hat{\mathbf{x}}, \quad (4)$$

such that (h_z,h_x,Ω) are constants, where $\Omega = \omega\tilde{\chi}_\perp^0/|\gamma|$ is the dimensionless driven frequency. We remark that due to the fact that the last term of the effective field (3) is proportional to $\mathbf{m}$, it is only incorporated in the term proportional to $\alpha_\parallel$ of Eq. (1).

The temperature-dependent parameters in the mean-field approximation

In order to use the LLB model, one needs to specify the temperature dependence of the susceptibility, the dissipative parameters $\alpha_\perp(T)$ and $\alpha_\parallel(T)$, and the equilibrium magnetization m_e. Their values can be obtained from experimental measurements. They can also be estimated from a multiscale approach (*ab initio* and atomistic) [47,58]. In this paper, for simplicity, we obtained their values under the mean-field approximation (MFA) previously used in the literature [41,42,53,59]. In this approximation, the static magnetization in equilibrium is taken from the Curie-Weiss law $\mathcal{M} = B[\beta(\mathcal{M}J_0 + \mu H_0)]$ at zero field, where $B(y) = \coth(y) - 1/y$ is the Langiven function, μ is the atomistic magnetic moment, J_0 is the strength of the exchange field, $\beta = 1/k_BT$, and k_B is the Boltzmann constant. Hence, the equilibrium magnetization m_e in Eq. (3) is given by $m_e = \mathcal{M}(H_0\to 0)$. Consequently, the longitudinal susceptibility is given by $\chi_\parallel = \partial\mathcal{M}/\partial H_0$, which at zero field can be cast in the form [39]

$$\tilde{\chi}_\parallel = \chi_\parallel(T,H_0)|_{H_0=0} = \frac{\mu}{J_0}\frac{\beta J_0 B'|_{H_0=0}}{1-\beta J_0 B'|_{H_0=0}}, \quad (5)$$

where $B'(y)\equiv dB(y)/dy$ and $f|_\zeta$ represents the function f evaluated at ζ. On the other hand, the perpendicular susceptibility $\tilde{\chi}_\perp(T)$ is assumed to be related to the anisotropy $K(T)$ through the relation [39]

$$\tilde{\chi}_\perp(T) = \frac{M_s^0 m_e(T)}{2K(T)}, \quad (6)$$

TABLE I. Simulational parameters. Values are taken close to that for Ni-based alloys from Ref. [59]. Here, $\mu_B = 9.27401 \times 10^{-24}$ A m^2.

T_C (K)	K_0 (J/m^3)	μ (μ_B)	M_S^0 (A/m)	$\tilde{\chi}_\perp^0$ (A m^2/J)
630	5.30×10^3	0.61	4.80×10^5	45.28

such that the anisotropic parameter is modeled by $K(T) = K_0 m_e^\eta(T)$, where $K_0 = K(T = 0)$ is the anisotropy constant at zero temperature and η is a material-specific scaling exponent. For uniaxial-anisotropy materials, we assume $\eta = 3$, which corresponds to the Callen-Callen theory [60]. For J_0, one can use a phenomenological relationship with the Curie temperature. For example, for a simple cubic lattice in the MFA, $J_0 = 3k_B T_C$ [39].

This effectively rewrites the MFA in terms of the T_C parameter and makes temperatures closer to the experimentally ones.

Finally, we consider the damping coefficients $\alpha_\perp$ and $\alpha_\parallel$ in the classical approximation given by [39]

$$\alpha_\perp(T) = \alpha_0\left(1 - \frac{T}{3T_C}\right), \tag{7}$$

and

$$\alpha_\parallel(T) = \alpha_0 \frac{2T}{3T_C},$$

where α_0 is the transverse damping coefficient at null temperature [38]. The typical values of this damping coefficient range from 10^{-3} to 10^{-1} (Ref. [10]). In addition, we remark that the longitudinal time scale of the LLB equation depends on the specific magnetic material, but is typically of the order of, or below, 1 ps. The typical orders of magnitude of the magnetic field components, H_j, range from 10^3 to 10^4 A/m, while the order the magnitude of the driven frequency is $\omega \sim 10^0$ GHz. The order of magnitude of the temperature ranges from 10^0 to 10^3 K. The set of parameters used in the simulations is summarized in Table I.

III. SIMULATIONS

This section is divided into two parts. In the first section, we briefly present the characterization techniques we used for analyzing the dynamical behavior of our system, and in the second one, we present and discuss our results.

A. Techniques of dynamics characterization

To characterize the dynamics described by the LLB equation, we will mainly use Lyapunov exponents (LEs). This method consists of quantifying the divergence between two initially close trajectories of a vector field [61]. In general, for an effective N-dimensional dynamical system described by a set of equations, $dX^i/d\tau = F^i(\mathbf{X},\tau)$, the ith Lyapunov exponent is given by

$$\lambda_i = \lim_{\tau\to\infty}\left[\frac{1}{\tau}\ln\left(\frac{\|\delta X_\tau^i\|}{\|\delta X_0^i\|}\right)\right], \tag{8}$$

where $\|\delta X_\xi^i\|$ is the distance between the trajectories of the ith component of the vector field at time ξ. These exponents can be ordered from the largest to the smallest as $\lambda_1 \geqslant \lambda_2 \geqslant \cdots \geqslant \lambda_N$. The first exponent is the largest Lyapunov exponent (LLE). Due to the fact that the applied magnetic field is time dependent, the effective dimension of the phase space of our system is four. Thus, from a dynamical system point of view, the LLE and the second largest LE (SLLE) may become positive, and therefore, by exploring the dependence of the LLE on the different parameters of the system, one can identify areas in the parameter space where the dynamics is chaotic (LLE positive) and others showing nonchaotic dynamics (LLE vanishing or negative). When both LLE and SLLE are positive, the system exhibits a *hyperchaotic* state [62–65]. This type of chaotic state appears in a dynamical system with minimal dimension four, so that it becomes more frequent for higher-dimensional systems. This feature indicates the possibility to have a complex attractor since more than one direction is expanded. In some cases, a hyperchaotic system can have two or multiple time scales. The first model of a hyperchaotic system was proposed by Rösler in 1979 [62]. The hyperchaotic states have been experimentally observed in electric circuits [66], chemical reactions [67], as well as optical devices [68], but not magnetic systems. On the other hand, let us comment that since we are dealing with a one-frequency forced system, at least one of its Lyapunov exponents is always zero, and hence the simplest attractor is a periodic orbit. Let us recall that this method has been widely used in different branches of physics and is considered one of the most effective approaches to quantify chaotic systems [61,69–71].

To analyze the dynamics of our system, we integrated Eq. (1) in the Cartesian representation by using a standard fourth-order Runge-Kutta integration scheme with a fixed time step $d\tau = 10^{-4}$. The LEs are calculated for a time span of $\tau = 2^{16}$ after disregarding an initial transient time $\tau = 10^4$. The Gram-Schmidt orthogonalization process [72] is performed after every $\delta\tau = 1$. This method is performed for orthonormalizing a set of vectors in an inner product space, and ensures the convergence of the LEs [61]. The error E in the evaluation of the LEs has been obtained by using $E = \sigma(\lambda_M)/\max(\lambda_M)$, where $\sigma(\lambda_M)$ is the standard deviation of the maximum positive LE. In all cases that we reported here, E is of the order of 1%, which is sufficiently small for the purpose of the present analysis.

B. Numerical results

Numerical simulations have been performed for particles with parameters presented in Table I. Due to the large number of control parameters, we have fixed the amplitude of the constant magnetic field at $h_z = 0.1$. The main results are depicted in Figs. 1–8.

In all cases, one of the Lyapunov exponents is zero, since one of the exponents belongs to the parametric forcing. Figure 1 shows the three other LEs as a function of a magnetic field h_x for three different temperatures, represented by solid, dotted, and dashed lines. In Fig. 1(a), $T/T_c = 0.0$ (LLG limit), we observe that the chaotic state starts at $h_x = 0.82$. For higher fields, the system exhibits multiple nonperiodic transitions between chaotic and regular behavior defined by $\lambda_M = 0.0$.

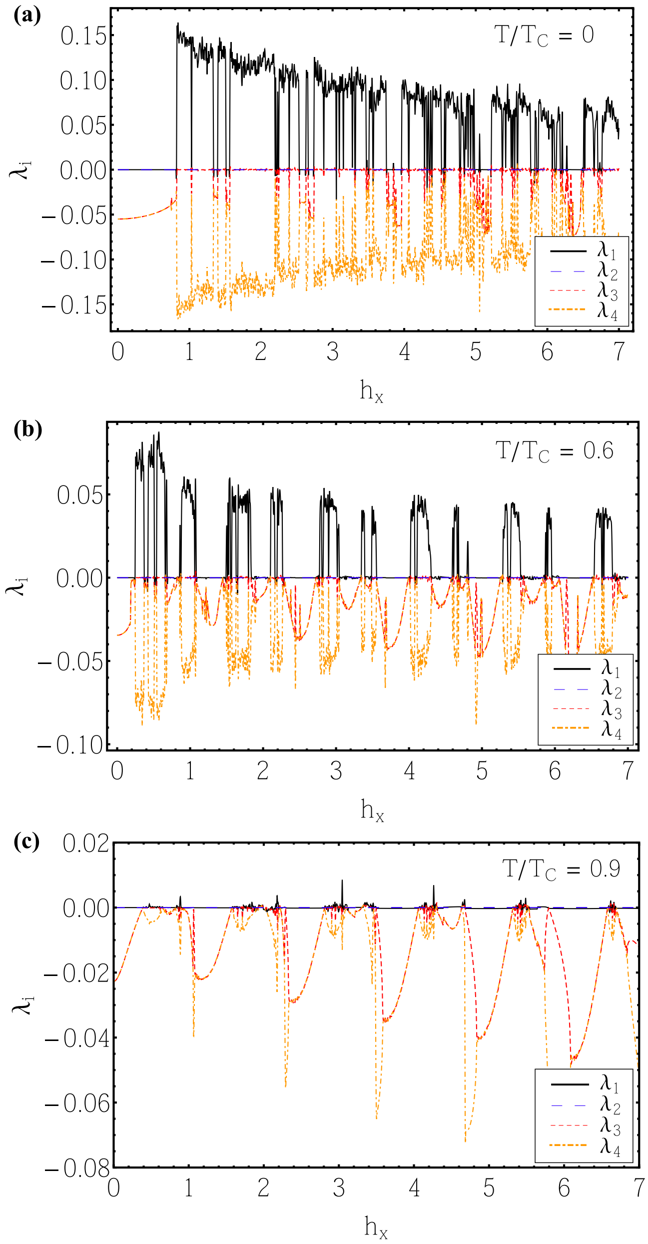

FIG. 1. LEs as a function of the field amplitude h_x for three different temperatures: (a) $T = 0$, (b) $T = 0.6T_C$, and (c) $T = 0.9T_C$. The fixed parameters are $\Omega = 0.4$, $h_z = 0.1$, and $\alpha_0 = 0.05$. The resolution in h_x is $\Delta h_x = 7.0 \times 10^{-3}$. The physical values of the parameters are $T_C = 630$ K, $\omega = 1.55$ GHz, and $H_z = 1679$ A/m.

At this temperature, the amplitude of the LLE inside the chaotic region decreases when the field increases. As shown in Fig. 1(b), at intermediate values of the temperature, the chaotic behavior starts at lower values of the field, $h_x = 0.25$, as compared to the previous case. Also the temperature modifies the dynamic states, decreasing the number of transitions between chaotic and regular regions. Therefore, some regions, that at zero temperature exhibit a chaotic behavior, with temperature present a regular dynamic, and vice versa. For higher temperatures, the regions that exhibit chaotic states almost disappear, as it is shown in Fig. 1(c). In addition, the numerical value of the positive LLE that characterizes

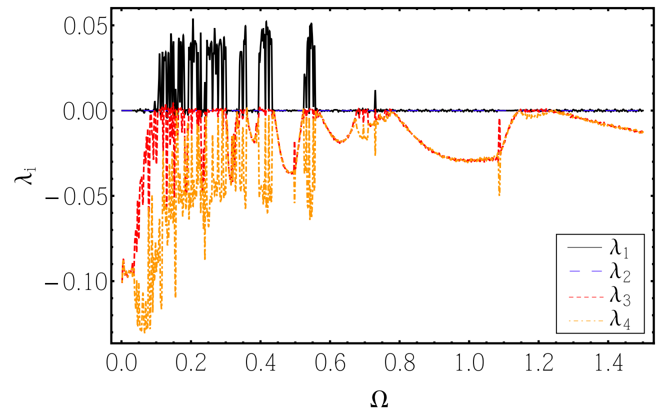

FIG. 2. Lyapunov exponents as a function of the frequency Ω. The continuous line depicts the largest Lyapunov exponent, while the dashed lines represent the lower Lyapunov exponents. For the results, we used $T = 0.6T_C$, $h_x = 3.0$, $h_z = 0.1$, and $\alpha_0 = 0.05$. The resolution in Ω is $\Delta\Omega = 2.0 \times 10^{-3}$. The physical values of the parameters are $T_C = 630$ K, $H_x = 52\,712$ A/m, and $H_z = 1679$ A/m.

the chaotic regime is quite small. Finally, we remark that for temperatures very close to the Curie temperature, the dynamical states are purely regular, independent of the field's value. We believe that the reason for this is that at high temperatures, the effect of longitudinal relaxation increases (due to the critical slowing-down effect [41,42,44]) and the dynamics becomes purely relaxational while the chaotic dynamics comes mostly from the precessional effect.

Figure 2 shows the Lyapunov exponents as a function of the frequency, Ω, at an intermediate temperature, $T = 0.6T_C$. From this figure, we observe that the system exhibits a regular behavior for frequencies lower than $\Omega \simeq 0.106$ and larger than $\Omega \simeq 0.732$. Between these two frequencies, the system is in a mixed regime, alternating between chaotic and regular

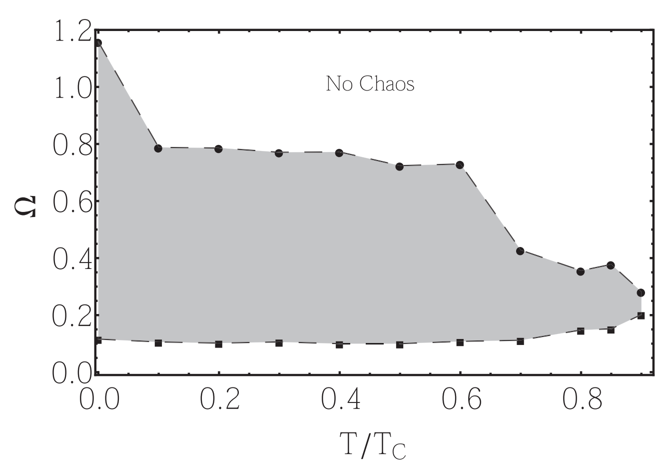

FIG. 3. Frequency thresholds of the region that exhibit a mixed behavior of the Lyapunov exponents, i.e., switching on and switching off of the chaotic states as a function of the the reduced temperature T/T_C. The squares and dots denote the lower and higher threshold, respectively. The gray area represents the mixed states from chaotic to regular states. The other fixed parameters are the same as used in Fig. 2.

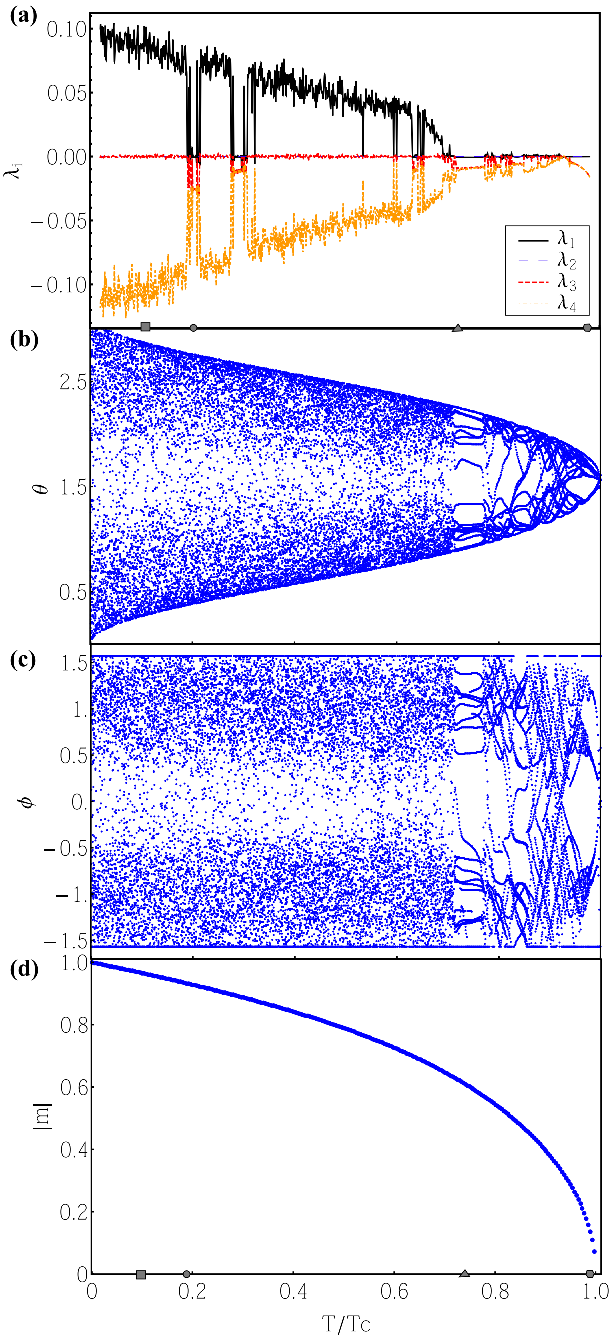

FIG. 4. (a) Lyapunov exponents λ_i as a function of the reduced temperature T/T_C. Bifurcation diagrams as a function of the reduced temperature T/T_C for the angular variables (b) θ, (c) ϕ, and (d) the module $|\mathbf{m}|$. The fixed parameters are $h_z = 0.1$, $h_x = 3.0$, $\Omega = 0.4$, and $\alpha_0 = 0.05$. The resolution in T/T_C is $\Delta T = 1.0 \times 10^{-3} T_C$. The physical values of the parameters are $T_C = 630$ K, $H_x = 52\,728$ A/m, $H_z = 1679$ A/m, and $\omega = 1.55$ GHz.

regimes. In the following, the frequencies separating the region between a purely regular behavior and a mixed state will be called thresholds. Figure 3 shows a phase diagram as a function of Ω and T/T_C such that the white area identifies the nonchaotic regimes, while the gray one contains both types of states. We can observe that the upper thresholds strongly depend on the temperature, leading us to conclude that for higher values of the temperature, this critical value of the frequency decreases. However, the lower limit of the mixed state is less dependent on the temperature.

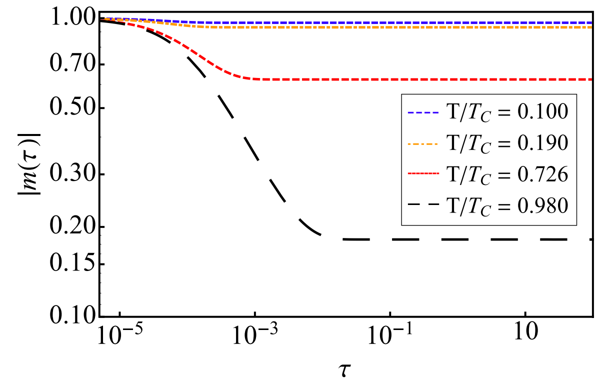

FIG. 5. Decay on time of the module $|\mathbf{m}|$ to the value of equilibrium as a function of the time, for four different temperatures. The fixed parameters are the same as Fig. 4.

In order to investigate in more detail the different dynamical states, we use other numerical techniques such as the computation of bifurcation diagrams, phase portraits, and Fourier power spectra [15,19–21,69,70]. Bifurcation diagrams have been previously used to quantify the nonperiodic behavior of a dynamical system [21,25]. Our bifurcation diagrams are obtained by repeatedly taking the maximum value of the time series of the spherical variables $\{m,\theta,\phi\}$, related by $\mathbf{m} = m(\cos\phi\sin\theta, \sin\phi\sin\theta, \cos\theta)$.

Figure 4 shows the dependence of the LEs, of the bifurcation diagrams of the angular variables $\{\theta,\phi\}$, and of the module of magnetization m of the reduced temperature, extracted from this technique. In the bifurcation diagrams when there is a continuum of points in the variable, the behavior can be multiperiodic, quasiperiodic, or chaotic. Hence, to discriminate complex regular states from chaotic ones, we need to compare these results with the LEs. From the LEs, one can observe that there are multiple transitions among chaotic and regular states and that for higher values of the temperature ($T > 0.7T_C$), the chaos is almost suppressed. In addition, the angular bifurcation diagrams show that the regular states are not simple periodic ones, since the maxima values are spread in the whole range of $\{\theta,\phi\}$ even when the LLE is null. There are some special cases where the angular variables are compacted in the diagram, such as in the region $T/T_C \in (0.701, 0.770)$. Moreover, we can observe that for higher temperatures, the regular states become multiperiodic ones.

On the other hand, from the bifurcation diagram for m, we can observe that its stationary modulus decreases when the temperature increases, resembling the equilibrium magnetization curve and following the law $m \cong a(1 - T/T_c)^p$ with $a = 1.02$ and $p = 0.39$. Also, we can observe that all the maxima in the time series have the same value, indicating that this variable has a pure relaxation dynamics for any type of the magnetization dynamical state, as shown in Fig. 5. In this figure, one can obverse that the modulus m tends fast to its equilibrium value m_e.

To have more insight into the dynamics of the system, we will analyze four values of the temperature, denoted by a

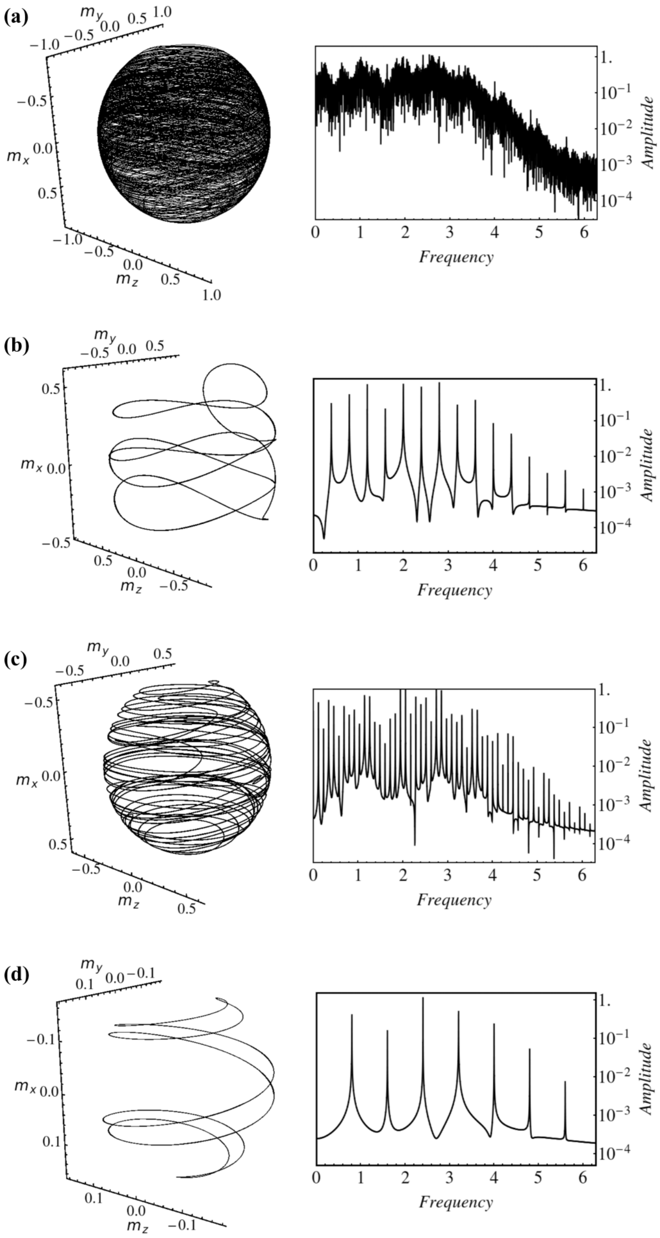

FIG. 6. Phase diagrams and Fourier power spectra for different temperatures: (a) $T/T_C = 0.1$, (b) $T/T_C = 0.19$, (c) $T/T_C = 0.726$, and (d) $T/T_C = 0.98$. These points are denoted on the diagrams of Fig. 4 with a square, circle, triangle, and hexagon, respectively.

square, a circle, a triangle, and a hexagon on Fig. 4(d). Figure 6 illustrates the tridimensional phase portrait and the Fourier power spectra of m_z for these four particular temperature values. In Fig. 6(a) at $T = 0.1T_C$, and because the LLE is positive ($\lambda_{\max} = 0.1$), the system exhibits a chaotic behavior. We observe that the trajectory of the magnetic moment fills the phase space, and the Fourier spectra shows a *continuum* set of characteristic frequencies. In Figs. 6(b)– 6(d), and because the LLE is vanishing, the system exhibits regular states. Nevertheless, these four regular states are quite different from each other. For instance, in Figs. 6(b) and 6(d), the particle describes multiperiodic behaviors since the Fourier spectra shows a discrete rational number of frequencies. We can also

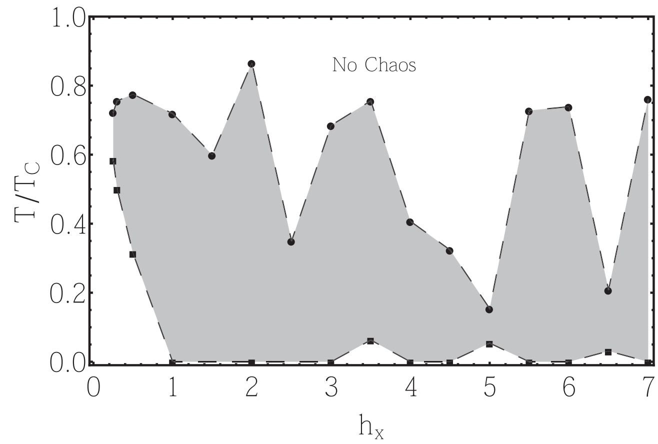

FIG. 7. Thresholds for switch on and switch off of the chaotic states as a function of the field amplitude, h_x, and the reduced temperature, T/T_C. The squares and dots denote the lower and higher threshold, respectively. The gray area represents the mixed states from chaotic to regular states. The fixed parameters are $h_z = 0.1$, $\Omega = 0.4$, and $\alpha = 0.05$. The physical values of the parameters are $H_z = 1679$ A/m and $\omega = 1.55$ GHz.

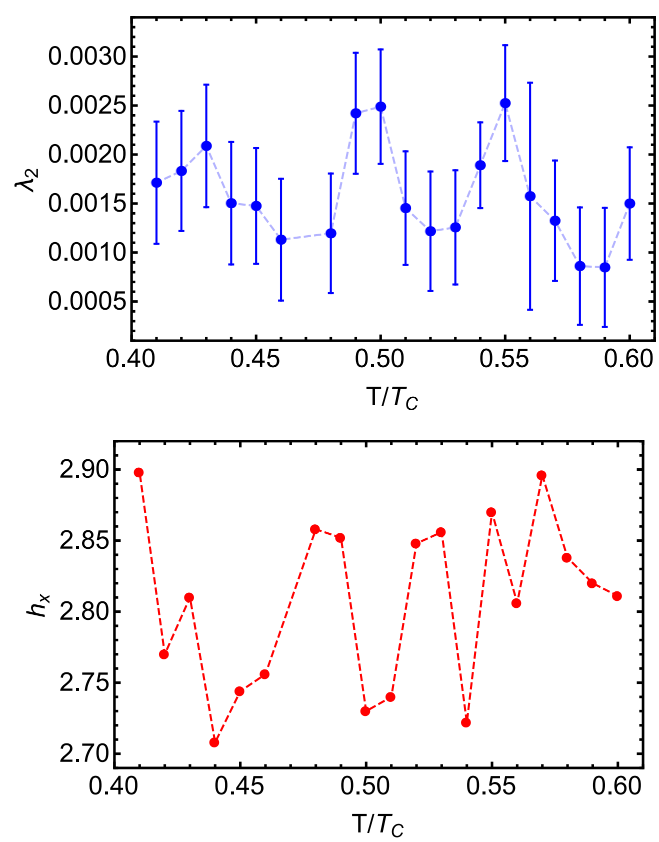

FIG. 8. Top: Second-largest Lyapunov exponents (SLLEs) a function of the temperature-reduced temperature, T/T_C. Bottom: Phase diagram of the occurrence of SLLEs as a function of h_x, and the reduced temperature, T/T_C. The fixed parameters are $h_z = 0.1$, $\Omega = 0.4$, and $\alpha = 0.005$. The physical values of the parameters are $H_z = 1679$ A/m and $\omega = 1.55$ GHz.

observe that in these two cases, the trajectories in the phase space are closed. Figure 6(c) corresponds to a regular state too, but in this case the behavior is a complex quasiperiodic one. In fact, from the Fourier spectra, one can observe that there are multiple modes and the ratio among them is irrational.

In addition, we compute the lower and higher thresholds of regular states as a function of the temperature and amplitude of the driving field, which are represented in Fig. 7. One can observe that the higher threshold follows a nonperiodic pattern, but the lower one is almost constant.

Finally, let us comment that due to the extra degree of freedom in the LLB, the possibility of finding two positive Lyapunov exponents exist, and therefore hyperchaotic states can be found. These states are much less frequent than chaotic ones, and require at least an effective four-dimensional dynamical system [62]. Figure 8(a) shows positive second largest Lyapunov exponents as a function of the reduced temperature, T/T_C. They are given for specific values of the driven field as it is shown in Fig. 8(b). We can observe that the numerical values of the SLLEs are small, but cannot be disregarded, as it is shown from the error bars. In addition, we can observe that the occurrence of hyperchaotic states is really reduced in the parameter space of this system.

IV. CONCLUSIONS

In conclusion, we have analyzed numerically the dynamics of an anisotropic magnetic particle in the presence of a time-dependent magnetic field using the Landau-Lifshitz-Bloch equation as a function of temperature, field amplitude, and frequency. Through the use of Lyapunov spectra, we observed that the system presents multiples transitions between chaotic and regular states as a function of these parameters. We also found that the upper limit between the regions of regular and mixed behaviors presents a strong temperature dependence. In fact, when the temperature increases, the frequency space of the chaotic region decreases, almost disappearing at temperatures near T_C. We also found that the modulus of the magnetization decreases when the temperature increases following a power law, and that this longitudinal variable presents pure relaxation dynamics irrespective of the general dynamical behavior of the magnetization. In addition, the system exhibits different types of regular states, being periodic with different periodicities or quasiperiodic for different temperatures. Finally, we have found a small set of the parameters where hyperchaotic dynamics is possible. This infrequent issue evidences that hyperchaos can exist in a single particle under an adequate combination of temperature and external driven field.

Finally, we believe that the control of different states via external parameters can be very useful for applications in spin-torque nano-oscillators and magnetic tunneling junctions. Indeed, the external frequency and/or ac field efficiently change the system response to states with very different spectral characteristics. For example, the change between chaotic and deterministic states via external parameter control can be potentially used as radio-frequency detectors, as has been suggested for the vortex-based magnetic tunneling junctions [36].

ACKNOWLEDGMENTS

We would like to thank P. Nieves (ICMM, CSIC, Spain) and R. L. Stamps (University of Glasgow, United Kingdom) for valuable discussions. In Chile, we acknowledge the partial support from a CONICYT-FONDECYT Postdoctoral fellowship, Grant No. 3130678, Fondecyt Grants No. 1120764 and No. 1160198, CONICYT-ANILLO ACT 1410, and the Basal Program through the Center for the Development to Nanoscience and Nanotechnology (Grant No. CEDENNA FB0807). We also acknowledge the support from the Spanish Ministry of Economy and Competitiveness under the Grant No. MAT2013-47078-C2-2-P. In Colombia, O.S. acknowledges the internal UniSucre Project No. 42-2015.

[1] Y. Acremann, C. H. Back, M. Buess, O. Portmann, A. Vaterlaus, D. Pesci, and H. Melchior, Imaging precessional motion of the magnetization vector, Science **290**, 492 (2000).
[2] Th. Gerrits, H. A. M. van den Berg, J. Hohlfeld, L. Bar, and Th. Rasing, Ultrafast precessional magnetization reversal by picosecond magnetic field pulse shaping, Nature (London) **418**, 509 (2002).
[3] B. Van Waeyenberge, A. Puzic, H. Stoll, K. W. Chou, T. Tyliszczak, R. Hertel, M. Fahnle, H. Bruckl, K. Rott, G. Reiss, I. Neudecker, D. Weiss, C. H. Back, and G. Schutz, Magnetic vortex core reversal by excitation with short bursts of an alternating field, Nature (London) **444**, 461 (2006).
[4] V. Uhlir, M. Urbanek, L. Hladik, J. Spousta, M.-Y. Im, P. Fischer, N. Eibagi, J. J. Kan, E. E. Fullerton, and T. Sikola, Dynamic switching of the spin circulation in tapered magnetic nanodisks, Nat. Nanotech. **8**, 341 (2013).
[5] E. Beaurepaire, J.-C. Merle, A. Daunois, and J.-Y. Bigot, Ultrafast Spin Dynamics in Ferromagnetic Nickel, Phys. Rev. Lett. **76**, 4250 (1996).
[6] Ju. Ganping, A. V. Nurmikko, R. F. C. Farrow, R. F. Marks, M. J. Carey, and B. A. Gurney, Ultrafast Time Resolved Photoinduced Magnetization Rotation in a Ferromagnetic/Antiferromagnetic Exchange Coupled System, Phys. Rev. Lett. **82**, 3705 (1999).
[7] A. V. Kimel, A. Kirilyuk, P. A. Usachev, R. V. Pisarev, A. M. Balbashov, and Th. Rasing, Ultrafast non-thermal control of magnetization by instantaneous photomagnetic pulses, Nature (London) **435**, 655 (2005).
[8] A. Kirilyuk, A. V. Kimel, and T. Rasing, Ultrafast optical manipulation of magnetic order, Rev. Mod. Phys. **82**, 2731 (2010).
[9] T. A. Ostler, J. Barker, R. F. L. Evans, R. W. Chantrell, U. Atxitia, O. Chubykalo-Fesenko, S. El Moussaoui, L. Le Guyader, E. Mengotti, L. J. Heyderman, F. Nolting, A. Tsukamoto, A. Itoh, D. Afanasiev, B. A. Ivanov, A. M. Kalashnikova, K. Vahaplar, J. Mentink, A. Kirilyuk, Th. Rasing, and A. V. Kimel, Ultrafast heating as a sufficient stimulus for magnetization reversal in a ferrimagnet, Nat. Commun. **3**, 666 (2012).

[10] G. Bertotti, I. Mayergoyz, and C. Serpico, *Nonlinear Magnetization Dynamics in Nanosystems* (Elsevier, Amsterdam, 2009).
[11] C. Thirion, W. Wernsdorfer, and D. Mailly, Switching of magnetization by nonlinear resonance studied in single nanoparticles, Nat. Mater. **2**, 524 (2003).
[12] G. Bertotti, I. D. Mayergoyz, C. Serpico, M. d'Aquino, and R. Bonin, Nonlinear-dynamical-system approach to microwave-assisted magnetization dynamics, J. Appl. Phys. **105**, 07B712 (2009).
[13] I. N. Krivorotov, N. C. Emley, R. A. Buhrman, and D. C. Ralph, Time-domain studies of very-large-angle magnetization dynamics excited by spin transfer torques, Phys. Rev. B **77**, 054440 (2008).
[14] G. Siracusano, G. Finocchio, A. La Corte, G. Consolo, L. Torres, and B. Azzerboni, Nonstationary magnetization dynamics driven by spin transfer torque, Phys. Rev. B **79**, 104438 (2009).
[15] L. F. Alvarez, O. Pla, and O. Chubykalo, Quasiperiodicity, bistability and chaos in the Landau-Lifshitz equation, Phys. Rev. B **61**, 11613 (2000).
[16] D. Laroze and P. Vargas, Dynamical behavior of two interacting magnetic nanoparticles, Phys. B **372**, 332 (2006).
[17] D. Laroze, P. Vargas, C. Cortes, and G. Gutierrez, Dynamics of two interacting dipoles, J. Magn. Magn. Mater. **320**, 1440 (2008).
[18] D. Laroze and L. M. Perez, Classical spin dynamics of four interacting magnetic particles on a ring, Physica B **403**, 473 (2008).
[19] D. I. Sementsov and A. M. Shutyi, Nonlinear regular and stochastic dynamics of magnetization in thin-film structures, Phys. Usp. **50**, 793 (2007).
[20] D. V. Vagin, and P. Polyakov, Control of chaotic and deterministic magnetization dynamics regimes by means of sample shape varying, J. App. Phys. **105**, 033914 (2009).
[21] R. K. Smith, M. Grabowski, and R. E. Camley, Period doubling toward chaos in a driven magnetic macrospin, J. Magn. Magn. Mater. **322**, 2127 (2010).
[22] Y. Khivintsev, B. Kuanr, T. J. Fal, M. Haftel, R. E. Camley, Z. Celinski, and D. L. Mills, Nonlinear ferromagnetic resonance in permalloy films: A nonmonotonic power-dependent frequency shift, Phys. Rev. B **81**, 054436 (2010).
[23] Y. Khivintsev, J. Marsh, V. Zagorodnii, I. Harward, J. Lovejoy, P. Krivosik, R. E. Camley, and Z. Celinski, Nonlinear amplification and mixing of spin waves in a microstrip geometry with metallic ferromagnets, Appl. Phys. Lett. **98**, 042505 (2011).
[24] G. Bertotti, C. Serpico, and I. D. Mayergoyz, Nonlinear Magnetization Dynamics under Circularly Polarized Field, Phys. Rev. Lett. **86**, 724 (2001).
[25] D. Laroze, J. Bragard, O. J. Suarez, and H. Pleiner, Characterization of the chaotic magnetic particle dynamics, IEEE Trans. Magn. **47**, 3032 (2011).
[26] J. Bragard, H. Pleiner, O. J. Suarez, P. Vargas, J. A. C. Gallas, and D. Laroze, Chaotic dynamics of a magnetic nanoparticle, Phys. Rev. E **84**, 037202 (2011)
[27] D. Laroze, D. Becerra-Alonso, J. A. C. Gallas, and H. Pleiner, Magnetization dynamics under a quasiperiodic magnetic field, IEEE Trans. Magn. **48**, 3567 (2012).
[28] L. M. Pérez, J. Bragard, H. L. Mancini, J. A. C. Gallas, A. M. Cabanas, O. J. Suarez, and D. Laroze, Anisotropy effects on magnetization dynamics, Netw. Heterog. Media **10**, 209 (2015).
[29] M. G. Phelps, K. L. Livesey, A. M. Ferona, and R. E. Camley, Tunable transient decay times in nonlinear systems: application to magnetic precession, Europhys. Lett. **109**, 37007 (2015).
[30] P.-B. He and W. M. Liu, Nonlinear magnetization dynamics in a ferromagnetic nanowire with spin current, Phys. Rev. B **72**, 064410 (2005).
[31] P. P. Horley, V. R. Vieira, P. M. Gorley, V. K. Dugaev, J. Berakdar, and J. Barnaś, Influence of a periodic magnetic field and spin-polarized current on the magnetic dynamics of a monodomain ferromagnet, Phys. Rev. B **78**, 054417 (2008).
[32] G. Gibson and C. Jeffries, Observation of period doubling and chaos in spin-wave instabilities in Yttrium Iron Garnet, Phys. Rev. A **29**, 811 (1984).
[33] F. M. de Aguiar, A. Azevedo, and S. M. Rezende, Characterization of strange attractors in spin-wave chaos, Phys. Rev. B **39**, 9448 (1989).
[34] J. Becker, F. Rodelsperger, Th. Weyrauch, H. Benner, W. Just, and A. Cenys, Intermittency in spin-wave instabilities, Phys. Rev. E **59**, 1622 (1999).
[35] J. Cai, Y. Kato, A. Ogawa, Y. Harada, M. Chiba, and T. Hirata, Chaotic dynamics during slow relaxation process in magnon systems, J. Phys. Soc. Jap. **71**, 3087 (2002).
[36] A. S. Jenkins, R. Lebrun, E. Grimaldi, S. Tsunegi, P. Bortolotti, H. Kubota, K. Yakushiji, A. Fukushima, G. de Loubens, O. Klein, S. Yuasa, and V. Cros, Spin-torque resonant expulsion of the vortex core for an efficient radiofrequency detection scheme, Nat. Nanotechnol. **11**, 360 (2016).
[37] *Chaos-based Cryptography: Theory, Algorithms and Applications*, edited by L. Kocarev and S. Lian (Springer-Verlag, Berlin, 2011).
[38] D. A. Garanin, Generalized Equation of motion for a ferromagnet, Physica A **172**, 470 (1991).
[39] D. A. Garanin, Fokker-Planck and Landau-Lifshitz-Bloch equations for classical ferromagnets, Phys. Rev. B **55**, 3050 (1997).
[40] P. Nieves, D. Serantes, U. Atxitia, and O. Chubykalo-Fesenko, Quantum Landau-Lifshitz-Bloch equation and its comparison with the classical case, Phys. Rev. B **90**, 104428 (2014).
[41] O. Chubykalo-Fesenko, U. Nowak, R. W. Chantrell, and D. Garanin, Dynamic approach for micromagnetics close to the Curie temperature, Phys. Rev. B **74**, 094436 (2006).
[42] U. Atxitia, O. Chubykalo-Fesenko, J. Walowski, A. Mann, and M. Münzenberg, Evidence for thermal mechanisms in laser-induced femtosecond spin dynamics, Phys. Rev. B **81**, 174401 (2010).
[43] C. Bunce, J. Wu, G. Ju, B. Lu, D. Hinzke, N. Kazantseva, U. Nowak, and R. W. Chantrell, Laser-induced magnetization switching in films with perpendicular anisotropy: A comparison between measurements and a multi-macrospin model, Phys. Rev. B **81**, 174428 (2010).
[44] J. Mendil, P. Nieves, O. Chubykalo-Fesenko, J. Walowski, T. Santos, S. Pisana, and M. Münzenberg, Resolving the role of femtosecond heated electrons in ultrafast spin dynamics, Sci. Rep. **4**, 3980 (2014).
[45] U. Kilic, G. Finocchio, T. Hauet, S. H. Florez, G. Aktas, and O. Ozatay, Magnetic switching driven by nanosecond scale heat and magnetic field pulses: An application of macrospin Landau-Lifshitz-Bloch model, Appl. Phys. Lett. **101**, 252407 (2012).

[46] C. Schieback, D. Hinzke, M. Kläui, U. Nowak, and P. Nielaba, Temperature dependence of the current-induced domain wall motion from a modified Landau-Lifshitz-Bloch equation, Phys. Rev. B **80**, 214403 (2009).

[47] N. Kazantseva, D. Hinzke, U. Nowak, R. W. Chantrell, U. Atxitia, and O. Chubykalo-Fesenko, Towards multiscale modeling of magnetic materials: Simulations of FePt, Phys. Rev. B **77**, 184428 (2008).

[48] D. Hinzke and U. Nowak, Domain Wall Motion by the Magnonic Spin Seebeck Effect, Phys. Rev. Lett. **107**, 027205 (2011).

[49] F. Schlickeiser, U. Ritzmann, D. Hinzke, and U. Nowak, Role of Entropy in Domain Wall Motion in Thermal Gradients, Phys. Rev. Lett. **113**, 097201 (2014).

[50] T. McDaniel, Application of Landau-Lifshitz-Bloch dynamics to grain switching in heat-assisted magnetic recording, J. Appl. Phys. **112**, 013914 (2012).

[51] C. Vogler, C. Abert, F. Bruckner, and D. Suess, Landau-Lifshitz-Bloch equation for exchange-coupled grains, Phys. Rev. B **90**, 214431 (2014).

[52] U. Atxitia, T. Ostler, J. Barker, R. F. L. Evans, R. W. Chantrell, and O. Chubykalo-Fesenko, Ultrafast dynamical path for the switching of a ferrimagnet after femtosecond heating, Phys. Rev. B **87**, 224417 (2013).

[53] O. J. Suarez, P. Nieves, D. Laroze, D. Altbir, and O. Chubykalo-Fesenko, Ultrafast relaxation rates and reversal time in disordered ferrimagnets, Phys. Rev. B **92**, 144425 (2015).

[54] R. F. L. Evans, D. Hinzke, U. Atxitia, U. Nowak, R. W. Chantrell, and O. Chubykalo-Fesenko, Stochastic form of the Landau-Lifshitz-Bloch equation, Phys. Rev. B **85**, 014433 (2012).

[55] W. F. Brown, Jr., Thermal Fluctuations of a Single-Domain Particle, Phys. Rev. **130**, 1677 (1963).

[56] J. L. García-Palacios and F. J. Lázaro, Langevin-dynamics study of the dynamical properties of small magnetic particle, Phys. Rev. B **58**, 14937 (1998).

[57] W. T. Coffey and Y. P. Kalmykov, Thermal fluctuations of magnetic nanoparticles - Fifty years after Brown, J. Appl. Phys. **112**, 121301 (2012).

[58] D. Hinzke, U. Atxitia, K. Carva, P. Nieves, O. Chubykalo-Fesenko, P. M. Oppeneer, and U. Nowak, Multiscale modeling of ultrafast element-specific magnetization dynamics of ferromagnetic alloys, Phys. Rev. B **92**, 054412 (2015).

[59] U. Atxitia, O. Chubykalo-Fesenko, N. Kazantseva, D. Hinzke, U. Nowak, and R. W. Chantrell, Micromagnetic modeling of laser-induced magnetization dynamics using the Landau-Lifshitz-Bloch equation, Appl. Phys. Lett. **91**, 232507 (2007).

[60] H. Callen and E. Callen, The present status of the temperature dependence of magnetocrystalline anisotropy and the $l(l+1)/2$ law, J. Phys. Chem. Solids **27**, 1271 (1966).

[61] A. Wolf, J. B. Swift, H. L. Swinney, and J. A. Vastano, Determining Lyapunov exponents from a time series, Physica D **16**, 285 (1985).

[62] O. E. Rössler, An equation for hyperchaos, Phys. Lett. A **71**, 155 (1979).

[63] Q. Jia, Hyperchaos generated from the Lorenz chaotic system and its control, Phys. Lett. A **366**, 217 (2007).

[64] D. Urzagasti, D. Becerra-Alonso, L. M. Pérez, H. L. Mancini, and D. Laroze, Hyper-chaotic magnetisation dynamics of two interacting dipoles, J. Low Temp. Phys. **181**, 211 (2015).

[65] D. Urzagasti, D. Becerra-Alonso, L. M. Pérez, H. L. Mancini, and D. Laroze, Hyper-chaotic and chaotic synchronisation of two interacting dipoles, Springer Proc. Phys. **173**, 261 (2016).

[66] T. Matsumoto, L. O. Chua, and K. Kobayashi, Hyperchaos: laboratory experiment and numerical confirmation, IEEE Trans. Circuit Syst. **33**, 1143 (1986).

[67] M. Eiswirth, Th.-M. Kruel, G. Ertl, and F. W. Schneider, Hyperchaos in a chemical reaction, Chem. Phys. Lett. **193**, 305 (1992).

[68] J.-P. Goedgebuer, L. Larger, and H. Porte, Optical Cryptosystem Based on Synchronization of Hyperchaos Generated by a Delayed Feedback Tunable Laser Diode, Phys. Rev. Lett. **80**, 2249 (1998).

[69] J. C. Sprott, *Chaos and Time-Series Analysis* (Oxford University Press, Oxford, 2003).

[70] J. A. C. Gallas, The structure of infinite periodic and chaotic hub cascades in phase diagrams of simple autonomous flows, Int. J. Bif. Chaos **20**, 197 (2010); and references therein.

[71] A. Sack, J. G. Freire, E. Lindberg, T. Pöschel, and J. A. C. Gallas, Discontinuous spirals of stable periodic oscillations, Sci. Rep. **3**, 3350 (2013).

[72] H. Gould and J. Tobochnik, *An Introduction to Computer Simulation Methods: Applications to Physical Systems*, 2nd ed. (Addison-Wesley, New York, 1996).